Journal of Materials Chemistry A

PAPER

View Article Online
View Journal | View Issue

Cite this: J. Mater. Chem. A, 2014, 2, 15829

Thermoelectric properties of Cu_3SbSe_3 with intrinsically ultralow lattice thermal conductivity†

Kriti Tyagi, Bhasker Gahtori, Sivaiah Bathula, A. K. Srivastava, A. K. Shukla, Sushil Auluck and Ajay Dhar*

Received 23rd May 2014
Accepted 17th July 2014

DOI: 10.1039/c4ta02590c

www.rsc.org/MaterialsA

We report the synthesis, characterization and evaluation of the thermoelectric properties of Cu_3SbSe_3 with a view to explore its utility as an useful thermoelectric material due to its intrinsically low thermal conductivity. Cu_3SbSe_3 was synthesized employing a solid state reaction process followed by spark plasma sintering, and the synthesized material was extensively characterized for its phase, composition and structure, which suggested formation of a single-phase. The measured electrical transport properties of Cu_3SbSe_3 indicated p-type conduction in this material. The electrical transport behavior agrees well with that predicted theoretically using first-principle density-functional theory calculations, employing generalized gradient approximation. The measured thermal conductivity was found to be 0.26 W m^{-1} K^{-1} at 550 K, which is the lowest reported thus far for Cu_3SbSe_3 and is among the lowest for state-of-the-art thermoelectric materials. Despite its ultralow thermal conductivity coupled with a moderate Seebeck coefficient, the calculated value of its thermoelectric figure-of-merit was found to be exceptionally low (<0.1), which was primarily attributed to its low electrical conductivity. Nevertheless, it is argued that Cu_3SbSe_3, due its environmentally-friendly constituent elements, ultralow thermal conductivity and moderate thermopower, could be a potentially useful thermoelectric material as the power factor can be favorably tailored by tuning the carrier concentration using suitable metallic dopants.

1. Introduction

Thermoelectric devices can play an important role in the generation of green energy, and hence, this technology is rapidly emerging as an alternative to other existing renewable sources of energy.[1–3] The efficiency of a thermoelectric device is mainly determined by the material's dimensionless figure-of-merit, $ZT = (\alpha^2\sigma/\kappa)T$, where α, σ, T and κ are the Seebeck coefficient, electrical conductivity, absolute temperature and total thermal conductivity, respectively. Further κ consists of contributions both from electronic (κ_e) and lattice (κ_L) parts ($\kappa = \kappa_L + \kappa_e$). Clearly ZT can be enhanced either by increasing the power factor ($\alpha^2\sigma$) or decreasing κ, although concurrently altering both of these parameters favorably would be the ideal situation. It has been experimentally established that in order to enhance ZT, reducing κ has been found to be a more experimentally plausible strategy and has been successfully demonstrated for several thermoelectric materials. Different reported proof-of-principle studies in this direction include synthesis of parent nano-crystalline materials,[4] *in situ* formation of nanoscale dots,[5] precipitation of nano-phases,[6] and artificially introduction of nano-particles.[7] As is clearly evident, most of these techniques involve some kind of nanostructuring-based approach, which, broadly speaking, can reduce κ_L by enhanced scattering of heat-carrying phonons[8–11] by the high density of nano-scale features of nearly comparable dimensions, apart from introducing some other favorable effects. However, if the resulting size of the nano-features, which generally arise as a result of nano-structuring, including grain boundaries, defects, and residual porosity, is very low (~10 nm), then these can also scatter electrons, thereby decreasing the electrical conductivity and nullifying the favorable effect of nanostructuring in enhancing ZT. In view of this, an alternative strategy is to develop thermoelectric materials with intrinsically low thermal conductivity, such as $AgSbTe_2$ ($\kappa \sim 0.39$ W m^{-1} K^{-1}, $ZT \sim 1.6$ at 673 K),[12] Ag_9TlTe_5 ($\kappa \sim 0.22$ W m^{-1} K^{-1}, $ZT \sim 1.2$ at 700 K),[13] $AgCrSe_2$ ($\kappa \sim 0.20$ W m^{-1} K^{-1}, $ZT \sim 1.0$ at 800 K)[14] and $Ag_{0.95}GaTe_2$ ($\kappa \sim 0.20$ W m^{-1} K^{-1}, $ZT \sim 0.7$ at 850 K).[15] The low thermal conductivity in these materials is primarily due to strong lattice anharmonicity caused by the presence of non-bonded valence electrons in the sp-hybridized bonding orbitals.[16,17] Recently, the ultralow thermal conductivity reported for thermoelectric SnSe ($\kappa \sim 0.23$ W m^{-1} K^{-1}, $ZT \sim 2.6$ at 973 K) has also been attributed to anharmonic and anisotropic bonding.[18] However, similar behavior is also observed in Cu–Sb–Se based ternary compounds, particularly Cu_3SbSe_3, which exhibits a very low thermal conductivity that is less than that of most of other

CSIR-Network of Institutes for Solar Energy, CSIR-National Physical Laboratory, Dr. K. S. Krishnan Marg, New Delhi-110012, India. E-mail: adhar@nplindia.org; Fax: +91-11-45609310; Tel: +91-11-45609456

† Electronic supplementary information (ESI) available. See DOI: 10.1039/c4ta02590c

chalcogenide-based thermoelectric compounds.[19] In Cu_3SbSe_3 compound, Sb is in +3 valence state, leaving two un-bonded 5s valence shell electrons (lone pairs). These electrons, due to their large polarizability, can give rise to strong anharmonicity (leading to strong phonon–phonon scattering) in Cu_3SbSe_3 resulting in their intrinsically low thermal conductivity.[20] Thus, the intrinsically low thermal conductivity in Cu_3SbSe_3, consisting of cost-effective elements, could be exploited for designing Cu_3SbSe_3 based efficient thermoelectric devices.

Surprisingly, despite its intrinsically low reported[17] κ and theoretically predicted $ZT \sim 0.7$,[21] there are no reports in the literature on its electrical transport and thermoelectric properties, although its electronic structure[22,23] and κ[17,24] have been investigated by several research groups. This seems to stem from the fact that it is difficult to synthesize single-phase Cu_3SbSe_3, and this synthesis has only been attempted by a few researchers.[17,25,26] However, several reports exist on the successful synthesis of its counterpart thermoelectric Cu_3SbSe_4.[27,28]

Do *et al.*[22] studied the underlying principles of band gap formation in both Cu_3SbSe_4 and Cu_3SbSe_3 and theoretically predicted the latter to be a better n-type thermoelectric material. Sevik and Çağin[21] calculated the thermoelectric properties of Cu_3SbSe_3 using density-functional theory (DFT) and Boltzmann transport theories and predicted a ZT of ~0.7 at 600 K for a p-type material. Similar theoretical calculations performed by Zhang *et al.*[23] suggest a positive value of the Grüneisen parameter, indicating a strong anharmonicity, and these authors found good agreement between their theoretically calculated κ and experimentally measured values reported previously.

Skoug *et al.*[17] reported the synthesis of Cu_3SbSe_3 employing directional fusion technique, but its single-phase formation was not substantiated by the authors, neither by X-ray diffraction (XRD) nor any other characterization data. However, these authors observed a low thermal conductivity due to strong anharmonic phonon interactions and complex crystal structure, for which it was thought to be a good thermoelectric material. Later, Kirkham *et al.*[25] also reported the synthesis of Cu_3SbSe_3 employing a vacuum melting technique but observed the presence of $CuSbSe_2$ and Cu_2Se phases in addition to the desired phase,[25] although they could finally obtain a single-phase material after subsequent heat-treatment for more than 72 hours. Recently, Liu *et al.*[26] also reported the colloidal synthesis of Cu_3SbSe_3 nano-crystals using a hot injection method, which is a multi-step chemical process. However, these authors have not reported the thermoelectric transport properties of these nanocrystals. Thus, it is apparent that although some efforts have been made towards synthesizing Cu_3SbSe_3, there are no reported experimental studies on their electrical transport or thermoelectric properties. In absence of these data, it is difficult to ascertain the previously reported utility of Cu_3SbSe_3 as a good thermoelectric material.[17]

In this paper, we present a comprehensive study on the synthesis, characterization and evaluation of the thermoelectric properties of Cu_3SbSe_3 synthesized using a solid-state reaction under vacuum followed by spark plasma sintering (SPS). The synthesized material was characterized for its phase, structure and composition employing XRD, field emission scanning electron microscopy (FESEM), high resolution transmission electron microscopy (HRTEM), energy dispersive X-ray spectroscopy (EDXS), X-ray photoelectron spectroscopy (XPS) and differential scanning calorimetry (DSC). The detailed characterization results clearly confirm the formation of Cu_3SbSe_3 in a single-phase, and the structure is in agreement with the previously reported results.[29] The electrical transport measurement results indicate that the as-synthesized Cu_3SbSe_3 shows a p-type behavior in the measured temperature range of 300–550 K. Electronic band structure of Cu_3SbSe_3 has been evaluated using first-principle DFT calculations, and the electrical transport properties were theoretically calculated using Boltzmann transport theory. These theoretical predicted values of α and σ were found to be in reasonable agreement with the experimental results. The measured κ was found to be 0.26 $W\,m^{-1}\,K^{-1}$ (550 K), which is the lowest value reported for this material. However, despite an ultralow κ and moderate value of α, the calculated ZT was abysmally low (<0.1) even at the highest temperature of measurement, which is contrary to the previously reported proposition.[21] Nevertheless, it is suggested that this material could possibly be a good potential thermoelectric material owing to its ultralow κ coupled with a reasonable value of α, as the power factor can be tailored favorably by tuning the carrier concentration using suitable metallic doping.[30,31]

2. Experimental details

High-purity Cu, Sb and Se powders were weighed in proper stoichiometric ratio and ground thoroughly in a glove-box under a high-purity argon atmosphere. The powders were subsequently pelletized and vacuum-sealed (10^{-4} Torr) in a quartz tube. The sealed quartz ampoule was placed in a box furnace and heat-treated at 320 °C for 96 h, and then the furnace was cooled to room temperature. This ingot was pulverized, and the resulting powder was consolidated and sintered under vacuum (~4 Pa) using SPS (SPS Syntex, 725) at a pressure of 60 MPa at 300 °C for 5 minutes (soaking time) at a heating rate of 300 °C min^{-1} using a cylindrical graphite die with a 12.7 mm central opening diameter to obtain cylindrical disks. Phase purity and its identification were carried out using XRD (Rigaku, Miniflex-II) with a CuK_α source with Ni filter. The XRD patterns were collected with a step size of 0.02° and scan rate of 2° per minute. HRTEM experiments were performed employing using a Tecnai G2 F30 STWIN operated at the electron accelerating voltage of 300 kV using electron source as field emission electron gun. Specimens for electron microscopy were prepared by employing mechanical polishing followed by subsequent ion milling. Mechanical polishing was finally carried out by thinning of a 3 mm diameter disc of specimen of about 50 to 100 μm down to a thickness of about 20 to 30 μm by utilizing a dimple grinder (model: 515 CE, South Bay Technology). Subsequently, ion beam milling was carried out by using an ion milling system (model: Baltec RES 101) at 7 kV and low angle milling to attain specimens that are electron beam transparent. During ion milling, Ar^+ ions were used for gentle thinning of the specimen without any damage for a few minutes. The density of the sample was measured using the

conventional Archimedes principle and was found to be 99% of its theoretical value. Thermal diffusivity measurements (Linseis, LFA 1000) were conducted on 12.7 mm diameter discs, and rectangular bars 10 × 3 × 3 mm were used for electrical transport measurements (Ulvac, ZEM 3) in the temperature range from room temperature to 600 K. Specific heat measurements were performed using a differential scanning calorimeter (Netzsch, DSC 404 F3). The accuracies in transport measurement were: ±6% for thermal diffusivity, ±10% for electrical conductivity, ±7% for the Seebeck coefficient, ±8% for specific heat and ±0.5% for density.

3. Computational details

The theoretical studies on Cu_3SbSe_3 are based on local density approximation (LDA) in DFT calculations. However, it has been reported earlier[32] that a significant improvement in the band structure is observed employing generalized gradient approximation (GGA) as compared to using LDA. We have employed the all-electron-full potential linearized augmented plane wave (FP-LAPW) method to calculate the electronic band structure, density of states and transport properties of Cu_3SbSe_3. The FP-LAPW method is based on DFT and is implemented in the WIEN2K code.[33] We treat $3d^{10}4s^1$, $5s^25p^3$, and $2s^22p^4$ as valence electrons in Cu, Sb, and Se atoms, respectively. The Cu_3SbSe_3 crystal structure used to carry out DFT calculations is orthorhombic (*Pnma*).[34] The structure is mainly composed by two types of framework, Cu–Se and Sb–Se, with the former providing the conduction path while the latter leads to distortion in the crystal symmetry. This complexity in crystal structure of Cu_3SbSe_3 would suggest a lower thermal conductivity.[35–37] The lattice constants and the atomic positions are taken from a ref. 34. Keeping the lattice constants fixed at the experimental values, we have optimized the atomic positions so that the force on each atom is 1 mRy per au. The optimization was done with 36 *k*-points in the Irreducible Brillouin Zone (IBZ), and self consistent DFT calculations were performed on the optimized structure of Cu_3SbSe_3 with a self-consistent field tolerance of 10^{-4} Ry. The electronic exchange–correlation energy was treated by the GGA of Perdew–Burke–Ernzerhof (PBE).[38] The self-consistency was obtained using 100 *k*-points in the IBZ. The total and the angular momentum decomposition of the atoms projected electronic density of states (DOS) were calculated using a mesh of 432 *k*-points. The transport properties were calculated employing the BoltzTraP code[39] using 6900 *k*-points in IBZ.

4. Results and discussion

The crystal structure of Cu_3SbSe_3 at room temperature was determined by conducting Rietveld refinement of the X-ray data using the FullProf program. Fig. 1 shows the XRD pattern of a Cu_3SbSe_3 sample at room temperature, along with its Rietveld refinement, which suggests that the sample is single-phase crystallized in an orthorhombic structure with *Pnma* (62) space group and lattice constant $a = 7.96$ Å, $b = 10.64$ Å, and $c = 6.81$ Å, which is in complete agreement with that reported earlier by

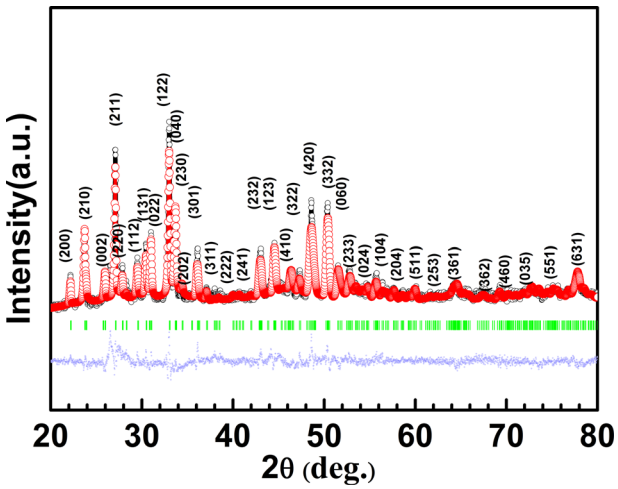

Fig. 1 XRD pattern of Cu_3SbSe_3 sample with Rietveld refinement. The red and black lines represent the observed and fitted data, respectively. The blue line represents the difference between the observed and fitted data.

Pfitzner.[29] The sharp peaks in the XRD pattern indicate high crystallinity in the synthesized sample, and the absence of any additional peaks suggests the phase purity of the synthesized Cu_3SbSe_3 sample. It may be noted that in the present study Cu_3SbSe_3 was synthesized at much lower temperatures using a solid-state reaction (320 °C) in vacuum followed by reaction sintering employing SPS (360 °C), in contrast to the only existing report in the literature by Skoug *et al.*[17] who employed a melting route (850 °C) followed by 72 hours of annealing.

A detailed microstructural characterization of Cu_3SbSe_3 samples employing HRTEM elucidated several interesting features in real and reciprocal space. A uniform microstructure is observed throughout the sample at low magnification (Fig. 2(a)). A grey-level contrast in the microstructure evolved due to grain boundaries as well as the difference in thickness between adjacent grains. However, these grains with a densely-packed microstructure were discerned throughout the material.

Inset A in Fig. 2(a) exhibits an atomic scale image of the encircled white-dotted region, which reveals the stacking of two set of planes arranged perpendicular to each set. The inter-

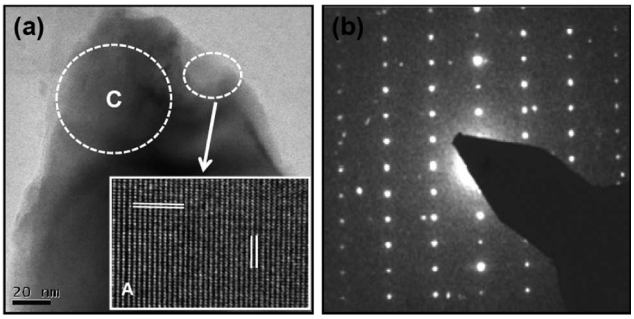

Fig. 2 HRTEM images of Cu_3SbSe_3, showing (a) a bright field electron micrograph of a uniform densely packed microstructure. Inset A shows an atomic scale image of white-dotted encircled region. (b) Selected area electron diffraction pattern of region C of (a).

planar spacings of these 200 and 040 planes are 0.39 and 0.27 nm, respectively, which corresponds to the Cu_3SbSe_3 orthorhombic crystal structure with lattice constants of $a = 0.79$, $b = 1.06$ and $c = 0.68$ nm and space group *Pnma* (62). The reciprocal space interpretation of the microstructure was performed by recording the selected area electron diffraction pattern (SAED) shown in Fig. 2(b), which clearly demonstrates this material to be of a single phase with good crystallinity. Moreover, a proper indexing exhibits that the diffraction pattern was oriented along the [001] zone axis of the orthorhombic crystal structure of Cu_3SbSe_3. A set of important planes, *hkl*: 040 and 200, are marked as diffraction spots 1 and 2, respectively, on the SAED (Fig. 2(b)).

An illustrative high resolution TEM micrograph, recorded at an atomic scale, displays a set of grains (marked as A to D in the inset of Fig. 3) with interfacing boundaries. This figure suggests that individual grains are randomly oriented with inter-planer spacings of 0.39, 0.33, 0.27, and 0.39 nm, corresponding to *hkl* values 200, 211, 040, and 200, for the grains marked from A to D, respectively (Fig. 3). However, at the grain boundaries, the structure appears to be either amorphous or crystallographically disturbed to some extent. For instance, on the interface between grains A and B, a clear amorphous phase is marked by a set of arrows. The amorphous region between the grains B to C is distinct with an average thickness of about 1.5 nm (marked with white dotted line). Boundaries between grains C and D and also between D and A are clearly marked by sets of arrows, due to mis-orientation of atomic planes among these respective grains (Fig. 3). The formation of amorphous grain boundaries of ~1–2 nm thickness are known to occur in several pristine compounds.[40,41] Fig. 3 further suggests that in some cases, the atomic scale imperfections are visible at some localized regions within an individual grain, which are clearly evident in grain A (encircled by white dotted lines). Similarly, in grain C, some lattice scale modulations are also apparent with a periodic spacing of about 1.2 nm.

The FESEM image of Cu_3SbSe_3 shown in Fig. 4 reveals a uniform, fine grained microstructure free from any visible residual porosity. The maximum densification post-sintering, achieved at a sintering temperature of 360 °C under a pressure of 60 MPa employing SPS, resulted in a densification of ~99%. This near-theoretical density is mainly due to the simultaneous application of pressure and a rapidly pulsated high DC current to the sample during SPS.[4,42,43]

The temperature dependences of the electrical and thermal transport parameters of Cu_3SbSe_3 are shown in Fig. 5. Fig. 5(a) shows the experimental temperature dependence of α for Cu_3SbSe_3 along with the theoretically predicted curves for different carrier concentrations. The positive value of the measured α indicates that the Cu_3SbSe_3 samples are p-type in nature. As is evident from Fig. 5(a), α increases nearly-linearly with temperature and attains a value of 190 $\mu V\ K^{-1}$ at 550 K. Fig. 5(b), which shows the variation of σ with temperature, also exhibits a nearly-linear dependence on temperature and shows a value of 1400 $S\ m^{-1}$ at 550 K, which is at least an order of magnitude lower than those observed for other state-of-the-art thermoelectric materials.[3] The low magnitude of σ may probably be due to its low carrier concentration, which was found to be 9.2×10^{19} cm^{-3}, when measured using a lab-made Hall apparatus at 300 K. However, the σ can be enhanced by incorporating suitable metallic dopants in Cu_3SbSe_3, which are known to migrate to form network of grain boundaries of the matrix microstructure.[44] Despite a nearly-linear temperature dependence of σ and α, a change in slope is clearly evident at ~450 K (Fig. 5(a) and (b)), which is attributed to the order–disorder transition in this material as reported earlier.[25] This transition is also clearly apparent with the temperature variation of specific heat, as shown in the inset of Fig. 5(c).

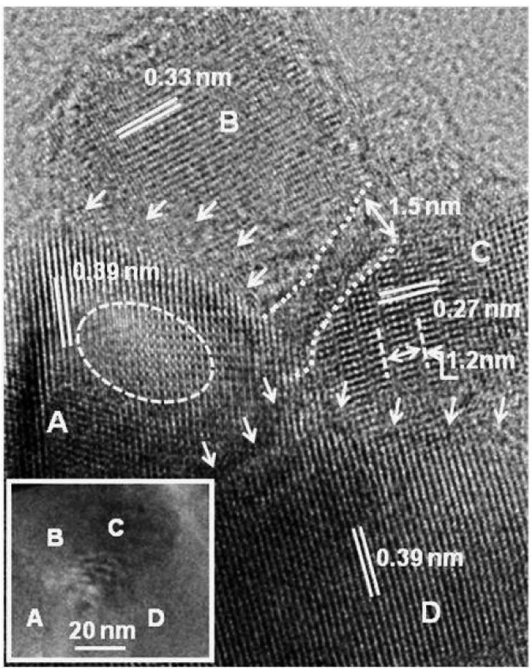

Fig. 3 HRTEM micrograph of Cu_3SbSe_3 showing different grains (A to D) with well defined crystallographic planes at an atomic scale. Inset: microstructure at low magnification, showing different grains.

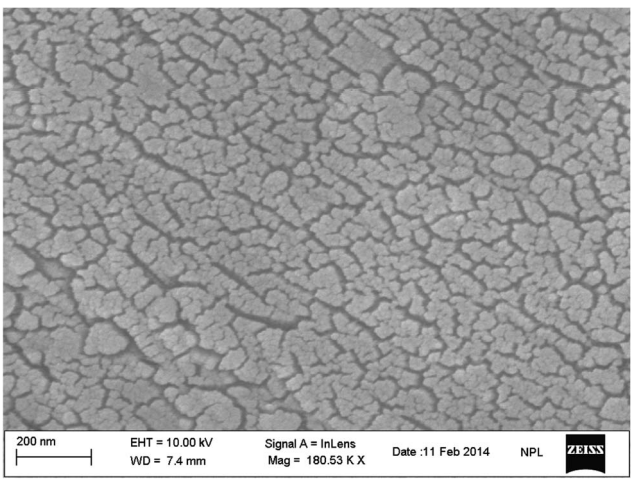

Fig. 4 SEM micrograph showing surface topography of as-synthesized Cu_3SbSe_3.

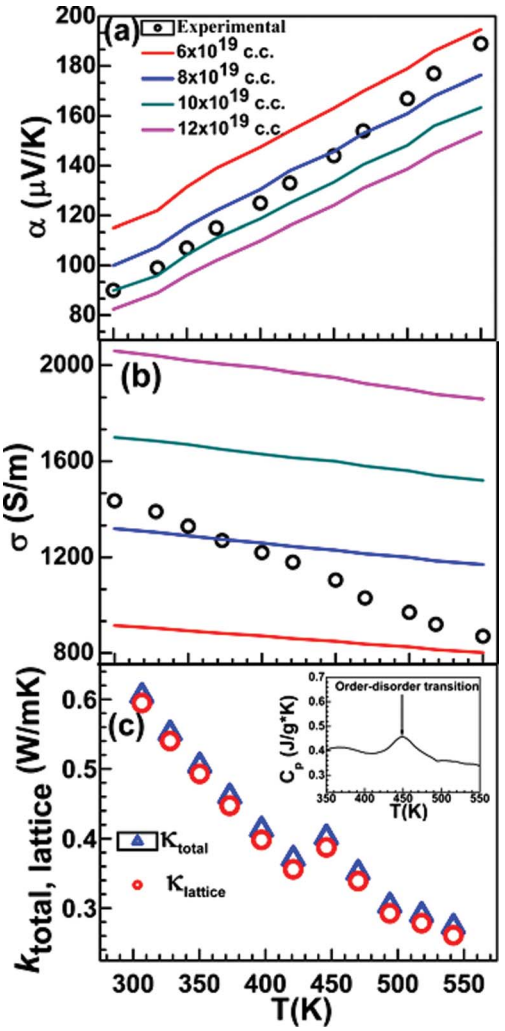

Fig. 5 Temperature dependence of transport properties of Cu_3SbSe_3. The open circles represent the experimental points, and the colored lines depict the theoretically predicted curves, for different carrier concentrations. (a) Seebeck coefficient, (b) electrical conductivity, and (c) total thermal conductivity. The inset shows the temperature dependence of C_p.

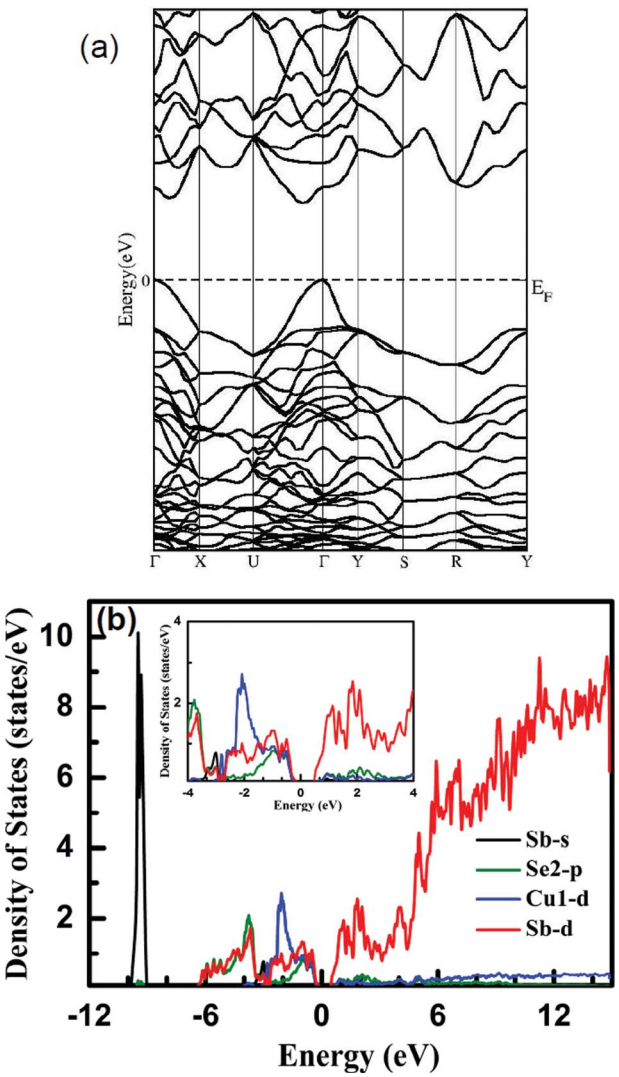

Fig. 6 (a) DFT results for band structure. The Fermi level is indicated by E_F and (b) the partial density of states as a function of energy. The inset shows a magnified view of this figure around the origin of the x-axis.

Fig. 5(c) represents the temperature dependence of κ and κ_L of Cu_3SbSe_3. κ_L has been extracted by subtracting κ_e from and κ_e, which was determined by using Wiedemann–Franz law $\kappa_e = L_0\sigma T$, where the Lorenz number $L_0 = 2.4 \times 10^{-8}$ W Ω K^{-2}. The temperature dependence of κ, as shown in Fig. 6(c), was found to be different than reported earlier by Kirkham *et al.*[25] for the same material, although a transition in C_p (inset) is clearly apparent at nearly the same temperature. Although the temperature variation of C_p is similar in the two studies, this discrepancy may be due to the difference in the temperature dependence of their thermal diffusivity, owing to the vastly different temperatures employed in their synthesis. The measured value of κ for our Cu_3SbSe_3 samples was found to be 0.60 W m^{-1} K^{-1} at 300 K, which is lower than the 0.7–1.0 W m^{-1} K^{-1} reported by earlier by Skoug *et al.*[17] However, at 550 K this value of κ for our Cu_3SbSe_3 sample was found to be 0.26 W m^{-1} K^{-1}, which is the lowest reported thus far for this material at this temperature. This ultralow value of κ in Cu_3SbSe_3 has previously been attributed to a combination of its complex crystal structure, very low Debye temperature and extreme anharmonicity of the lattice vibrational spectrum that gives rise to a large value Grüneisen parameter in this compound.[23] Owing to its ultralow κ, it was previously suggested that the Cu_3SbSe_3 compound could potentially be a good thermoelectric material.[17,21] It is further evident from Fig. 5 that κ is largely dominated by the phononic contribution with negligible contribution from the electronic part, as is generally the case for thermoelectric materials with intrinsically low thermal conductivity due to anharmonicity of the lattice phonons.[17,23]

The ZT, calculated using the measured α, σ and κ data for our Cu_3SbSe_3 compound, exhibits a very low value ZT (<0.1) in the entire measured temperature range, which is contrary to the previously reported proposition.[17,21] Nevertheless, this material could be a good potential thermoelectric material due to its ultralow κ coupled with a moderate value of α, as the power

factor can be tailored favorably by tuning the carrier concentration employing suitable metallic doping.[30,31] There have been several studies demonstrating how the transport phenomenon can be tuned by optimization of carrier concentration for further enhancement of *ZT* in existing high performance TE materials.[44–46] Kurosaki *et al.*[45] observed an enhancement in *ZT* of AgTlTe by tuning the carrier concentration *via* Cu doping. They observed a significant increase in the power factor in AgTlTe without increasing the κ by doping with 40% Cu, finally leading to a drastic increase in *ZT* from 0.3 to 0.6. Similarly the σ in Mg_2Si increases by several orders of magnitude upon metallic doping, resulting in an enormous increase in *ZT* by more than an order of magnitude.[31] The enhancement of the power factor of $AgGaTe_2$ through carrier concentration tuning has also been recently theoretically predicted[46] using density functional theory and Boltzmann transport theory. Several other strategies employed for the enhancement of the power factor leading to enhancement of *ZT* in PbTe-based systems have been summarized by Rawat *et al.*[44,47]

5. Computational results

Our GGA calculations show that Cu_3SbSe_3 is a semiconductor with an indirect band gap of 0.47 eV. The total and the angular momentum of the decomposition of the atoms' projected electronic density of states (DOS) were calculated using a mesh of 432 *k*-points. The transport properties were calculated with the BoltzTraP code[36] using 6900 *k*-points in IBZ.

The band structure is shown in Fig. 6(a). This compound shows an indirect energy gap of 0.47 eV located between Γ and *U*. Fig. 6(b) shows the partial density of states of Cu1-d, Se2-p, Sb-s and Sb-d. We find that the peak around −9 eV arises from the s-states of Sb. The inset of the figure shows the density of states on a smaller scale for more clarity. The top of the valence band has major contributions from Cu1-d, Se2-p and Sb-d, while the bottom of the conduction band arises from Sb-d states. We find a significant hybridization between Cu1-d, Se2-p and Sb-s from −3.0 eV to the top of the valance bands and Se2-p and Sb-s from −7.0 to −3.0 eV. The conduction bands are mainly of Sb-d character. Earlier theoretical calculations by Sevic and Çağin,[21] performed using LDA, agree with our findings, revealing an indirect band gap of 0.24 eV. Do *et al.*[22] also reported that Cu_3SbSe_3 is narrow indirect band gap semiconductor. The density of states curve shows a large slope at the band edges indicative of large α, which is reflected in our experimental findings (Fig. 5(a)).

To substantiate the above measurements of the transport properties, we also performed calculations of the transport properties using GGA and then compared them with experimental values. Fig. 5(a) shows the temperature dependence plots for both the measured and theoretically calculated α for different doping concentrations on the order of 10^{19} cm^{-3}. The open circles indicate the experimental values, while different lines show values of σ at different doping levels. We have plotted four different concentrations of α and σ calculations against temperature to determine which matches better. While performing calculations using BoltzTrap code, we assumed a temperature independent relaxation time and took the value of τ to be 10^{-14} s.[48] The graph shows that α increases with temperature for all of the samples over the entire temperature range for both the theoretical and experimental cases. The results show that the magnitude of α for experimental data points, which has a highest value of 189 $\mu V\ K^{-1}$ at 550 K, is in reasonable agreement with the calculated data plotted for different doping concentrations over the entire temperature range.

Fig. 5(b), which displays both the experimentally measured and theoretically predicted temperature dependence of σ, shows a pronounced decrease in σ with increasing temperature. The decrease in experimental σ could be attributed to the temperature dependence of τ, while for theoretically calculated value of τ is taken as a constant, which could explain the visible difference between the experimental and theoretical behavior of σ.

6. Conclusions

We present the first complete study on the synthesis, characterization and thermoelectric property evaluation of Cu_3SbSe_3. The material was synthesized employing a solid state reaction followed by spark plasma sintering, and its phase structure and composition were characterized using XRD, HRTEM, EDXS, SEM, XPS and DSC, which confirmed the formation of Cu_3SbSe_3 in a single-phase. The electrical transport measurements suggest that Cu_3SbSe_3 exhibits a p-type behavior with moderate Seebeck coefficient values (190 $\mu V\ K^{-1}$ at 550 K). The electrical conductivity and Seebeck coefficient, evaluated theoretically using first-principle DFT calculations, show reasonable agreement with the experimentally determined values. The measured thermal conductivity is observed to be 0.26 $W\ m^{-1}\ K^{-1}$ (at 550 K) and is the lowest reported for this material thus far, with the main contribution coming from the lattice part. Despite a very low value of measured thermal conductivity, the calculated *ZT* is found to be abysmally low (<0.1), which is due its low electrical conductivity. Nevertheless, due to the environmentally friendly constituent elements coupled with its ultralow thermal conductivity, Cu_3SbSe_3 could be a potential thermoelectric material, as its power factor can be enhanced by tuning the carrier concentration by employing suitable metallic dopants.

Acknowledgements

This work was supported by the CSIR-TAPSUN programme entitled "Novel approaches for solar energy conversion under technologies and products for solar energy utilization through networking – NWP54." The authors are grateful to the Director, Prof. R. C. Budhani, for his constant mentoring and support for this project. Thanks are also due to Prof. S. D. Mahanti for his valuable comments. The technical support rendered by Mr Radhey Shyam and Mr Naval Kishor Upadhyay is also gratefully acknowledged.

References

1 S. Ballikaya, H. Chi, J. R. Salvador and C. Uher, *J. Mater. Chem. A*, 2013, **1**, 12478–12484.

2 J. R. Sootsman, D. Y. Chung and M. G. Kanatzidis, *Angew. Chem., Int. Ed.*, 2009, **48**, 8616–8639.
3 G. J. Snyder and E. S. Toberer, *Nat. Mater.*, 2008, **7**, 105–114.
4 S. Bathula, M. Jayasimhadri, N. Singh, A. Srivastava, J. Pulikkotil, A. Dhar and R. Budhani, *Appl. Phys. Lett.*, 2012, **101**, 213902.
5 Y. K. Koh, C. Vineis, S. Calawa, M. Walsh and D. G. Cahill, *Appl. Phys. Lett.*, 2009, **94**, 153101.
6 L. P. Tan, T. Sun, S. Fan, R. V. Ramanujan and H. H. Hng, *J. Alloys Compd.*, 2014, **587**, 420–427.
7 W. Kim, J. Zide, A. Gossard, D. Klenov, S. Stemmer, A. Shakouri and A. Majumdar, *Phys. Rev. Lett.*, 2006, **96**, 045901.
8 L. Hicks, T. Harman and M. Dresselhaus, *Appl. Phys. Lett.*, 1993, **63**, 3230–3232.
9 M. Dresselhaus, G. Dresselhaus, X. Sun, Z. Zhang, S. Cronin and T. Koga, *Phys. Solid State*, 1999, **41**, 679–682.
10 J. P. Heremans, C. M. Thrush and D. T. Morelli, *Phys. Rev. B: Condens. Matter Mater. Phys.*, 2004, **70**, 115334.
11 L. Hicks and M. Dresselhaus, *Phys. Rev. B: Condens. Matter Mater. Phys.*, 1993, **47**, 12727.
12 H. Wang, J.-F. Li, M. Zou and T. Sui, *Appl. Phys. Lett.*, 2008, **93**, 202103–202106.
13 K. Kurosaki, A. Kosuga, H. Muta, M. Uno and S. Yamanaka, *Appl. Phys. Lett.*, 2005, **87**, 061919.
14 F. Gascoin and A. Maignan, *Chem. Mater.*, 2011, **23**, 2510–2513.
15 Y. Aikebaier, K. Kurosaki, T. Sugahara, Y. Ohishi, H. Muta and S. Yamanaka, *J. Mater. Sci. Eng. B*, 2012, **177**, 999–1002.
16 D. Morelli, V. Jovovic and J. Heremans, *Phys. Rev. Lett.*, 2008, **101**, 035901.
17 E. J. Skoug, J. D. Cain and D. T. Morelli, *Appl. Phys. Lett.*, 2010, **96**, 181903–181905.
18 L.-D. Zhao, S.-H. Lo, Y. Zhang, H. Sun, G. Tan, C. Uher, C. Wolverton, V. P. Dravid and M. G. Kanatzidis, *Nature*, 2014, **508**, 373–377.
19 T. P. Hogan, A. Downey, J. Short, J. D'Angelo, C.-I. Wu, E. Quarez, J. Androulakis, P. F. Poudeu, J. R. Sootsman and D.-Y. Chung, *J. Electron. Mater.*, 2007, **36**, 704–710.
20 Y. Lan, A. J. Minnich, G. Chen and Z. Ren, *Adv. Funct. Mater.*, 2010, **20**, 357–376.
21 C. Sevik and T. Çağın, *J. Appl. Phys.*, 2011, **109**, 123712.
22 D. Do, V. Ozolins, S. D. Mahanti, M.-S. Lee, Y. Zhang and C. Wolverton, *J. Phys.: Condens. Matter*, 2012, **24**, 415502.
23 Y. Zhang, E. Skoug, J. Cain, V. Ozoliņš, D. Morelli and C. Wolverton, *Phys. Rev. B: Condens. Matter Mater. Phys.*, 2012, **85**, 054306.
24 D. T. Do and S. Mahanti, *J. Phys. Chem. Solids*, 2014, **75**, 477–485.
25 M. Kirkham, P. Majsztrik, E. Skoug, D. Morelli, H. Wang, W. D. Porter, E. Andrew Payzant and E. Lara-Curzio, *J. Mater. Res.*, 2011, **26**, 2001.
26 Y. Liu, J. Yang, E. Gu, T. Cao, Z. Su, L. Jiang, C. Yan, X. Hao, F. Liu and Y. Liu, *J. Mater. Chem. A*, 2014, **2**, 6363–6367.
27 C. Yang, F. Huang, L. Wu and K. Xu, *J. Phys. D: Appl. Phys.*, 2011, **44**, 295404.
28 E. J. Skoug, J. D. Cain, P. Majsztrik, M. Kirkham, E. Lara-Curzio and D. T. Morelli, *Sci. Adv. Mater.*, 2011, **3**, 602–606.
29 A. Pfitzner, *Z. Anorg. Allg. Chem.*, 1995, **621**, 685–688.
30 Y. Pei, Z. M. Gibbs, B. Balke, W. G. Zeier and G. J. Snyder, *Adv. Energy Mater.*, 2014, DOI: 10.1002/aenm.201400486.
31 S. Muthiah, J. Pulikkotil, A. Srivastava, A. Kumar, B. Pathak, A. Dhar and R. Budhani, *Appl. Phys. Lett.*, 2013, **103**, 053901–053905.
32 C. Stampfl and C. Van de Walle, *Phys. Rev. B: Condens. Matter Mater. Phys.*, 1999, **59**, 5521.
33 P. Blaha, K. Schwarz, G. Madsen, D. Kvasnicka and J. Luitz, *Local Orbitals Program for Calculating Crystal Properties*, 2001.
34 A. Pfitzner, *Z. Anorg. Allg. Chem.*, 1994, **620**, 1992–1997.
35 G. A. Slack, *Solid State Phys.*, 1979, **34**, 1–71.
36 A. Zevalkink, E. S. Toberer, W. G. Zeier, E. Flage-Larsen and G. J. Snyder, *Energy Environ. Sci.*, 2011, **4**, 510–518.
37 E. S. Toberer, A. F. May and G. J. Snyder, *Chem. Mater.*, 2009, **22**, 624–634.
38 J. P. Perdew, K. Burke and M. Ernzerhof, *Phys. Rev. Lett.*, 1996, **77**, 3865.
39 K. Schwarz, P. Blaha and G. K. H. Madsen, *Comput. Phys. Commun.*, 2002, **147**, 71–76.
40 A. P. Tomsia and A. M. Glaeser, *Ceramic Microstructures: Control at the Atomic Level*, Springer, 1998.
41 L. Priester, *Grain Boundaries: From Theory to Engineering*, Springer, 2012.
42 S. Bathula, R. Anandani, A. Dhar and A. Srivastava, *J. Mater. Sci. Eng. A*, 2012, **545**, 97–102.
43 A. Bhardwaj, D. Misra, J. Pulikkotil, S. Auluck, A. Dhar and R. Budhani, *Appl. Phys. Lett.*, 2012, **101**, 169901–169903.
44 P. Rawat, B. Paul and P. Banerji, *Materials and processes for energy: Communicating current research and technological developments*, Formatex Research Center, 2013.
45 K. Kurosaki, K. Goto, H. Muta and S. Yamanaka, *J. Appl. Phys.*, 2007, **102**, 023707.
46 H. Peng, C. Wang and J. Li, *Phys. B*, 2014, **441**, 68–71.
47 P. K. Rawat, B. Paul and P. Banerji, *Phys. Status Solidi RRL*, 2012, **6**, 481–483.
48 N. Ashcroft and N. Mermin, *Solid State Physics*, Saunders College, Philadelphia, Pennsylvania, 1976.